Molecular dynamics simulation of the response of a gas to a spherical piston: Implications for sonoluminescence

Steven J. Ruuth,[1,*] Seth Putterman,[2] and Barry Merriman[3,†]
[1]*Department of Mathematics, Simon Fraser University, Burnaby, British Columbia, Canada V5A 1S6*
[2]*Department of Physics, University of California at Los Angeles, Los Angeles, California 90095-1547*
[3]*Department of Mathematics, University of California at Los Angeles, Los Angeles, California 90095-1555*
(Received 16 November 2001; published 20 September 2002)

Sonoluminescence is the phenomena of light emission from a collapsing gas bubble in a liquid. Theoretical explanations of this extreme energy focusing are controversial and difficult to validate experimentally. We propose to use molecular dynamics simulations of the collapsing gas bubble to clarify the energy focusing mechanism, and determine physical parameters that restrict theories of the light emitting mechanism. In this paper, we model the interior of a collapsing noble gas bubble as a hard sphere gas driven by a spherical piston boundary moving according to the Rayleigh-Plesset equation. We also include a simplified treatment of ionization effects in the gas at high temperatures. The effects of water vapor are neglected in the model. By using fast, tree-based algorithms, we can exactly follow the dynamics of 10^6 particle systems during the collapse. Our preliminary model shows strong energy focusing within the bubble, including the formation of shocks, strong ionization, and temperatures in the range of 50 000–500 000 K. Our calculations show that the gas-liquid boundary interaction has a strong effect on the internal gas dynamics, and that the gas passes through states where the mean free path is greater than the characteristic distance over which the temperature varies. We also estimate the duration of the light pulse from our model, which predicts that it scales linearly with the ambient bubble radius. As the number of particles in a physical sonoluminescing bubble is within the foreseeable capability of molecular dynamics simulations, we also propose that fine scale sonoluminescence experiments can be viewed as excellent test problems for advancing the art of molecular dynamics.

DOI: 10.1103/PhysRevE.66.036310 PACS number(s): 78.60.Mq, 02.70.Ns

I. INTRODUCTION

A. Background

As a gas bubble in a liquid collapses, the potential energy stored during its prior expansion is released and strongly focused. The extent of focusing can be so great that a burst of light is emitted at the final stage of collapse. This process can be driven repeatedly by exciting bubbles with a sound field, and the resulting transduction of sound into light is known as sonoluminescence (SL) [1–6].

Sonoluminescence can be observed in dense fields of transient cavitation bubbles produced by applying intense sound to a liquid, or in a periodic single bubble mode which allows more detailed experimental observations. In single bubble SL, a single gas bubble in the liquid is created and periodically driven to expand and collapse by an applied sound field. The bubble begins its cycle of evolution as the low pressure phase of the sound field arrives, causing it to expand to a maximal radius. As the applied acoustic pressure increases, the bubble begins to collapse, first reaching its ambient radius and corresponding ambient pressure and internal temperature, and then radially collapsing further, with the bubble walls falling inward driven by the rising external fluid pressure. The collapse accelerates rapidly, until gas trapped inside the bubble is compressed and heated to a pressure that ultimately halts and reverses the motion of the bubble walls. Thus the bubble reaches a minimum radius, and then rapidly ''bounces'' back to a much larger size. At some point near the minimum radius, the resulting internal ''hot spot'' can release a burst of light. While the basic bubble collapse dynamics can be observed for a variety of gas and liquid combinations, light emission typically requires the bubble to contain sufficient amount of a noble gas, and works particularly well in water.

The mechanism of light emission from the gas is not understood, not much is known about related quantities such as peak temperatures, pressures, or levels of ionization.

B. Limitations of hydrodynamic models

It is known that the mechanical conditions during collapse of a common gas bubble in water are quite extreme: as the bubble reaches submicron diameter, the bubble wall experiences accelerations that exceed $10^{11}g$ and supersonic changes in velocity that occur on picosecond time scales. In order to understand how this affects the state of the internal gas, the standard approach is to apply continuum fluid mechanics. Some models assume that pressure and temperature are uniform inside of the collapsed bubble [7] while other theories calculate the effects of imploding shock waves [6,8–10]. Various fluid models have been applied both at nondissipative (Euler equations) and dissipative (Navier-Stokes equations) levels of description [11–14].

All these fluid approaches are limited in their predictive power by the need to represent transport processes and the equation of state. Under such extreme flow conditions, little is known about these effects and one is forced to extrapolate from known forms. The net result is that the modeling pre-

*Email address: sruuth@sfu.ca
†Email address: barry@math.ucla.edu

dictions directly reflect these assumptions. This is not satisfactory for the purpose of understanding what actually occurs within the bubble.

An especially fundamental limitation of continuum mechanical approaches is the assumption of local thermodynamic equilibrium, i.e., it is assumed that the macroscopic fluid variables do not change much over molecular length and time scales. Although the bubble starts out in such a state, its subsequent runaway collapse ultimately leads to a regime where this clearly does not hold. In this state, from which the ultraviolet picosecond flash of light is emitted, one can question the basic applicability of hydrodynamic models.

C. Molecular dynamics modeling

We propose to remove the assumption of thermodynamic equilibrium, and also eliminate the controversy over the correct equation of state, by using molecular dynamics (MD) simulations of the gas dynamics within the bubble. In this approach, we directly apply Newton's laws of motion to the gas molecules, including as much detail as is desired (or practical) about the molecular collisions and related atomic physics. With the inclusion of sufficient detail and efficient programming, it could ultimately allow the simulation of the light emission process itself.

While the small length and time scales of sonoluminescence present major obstacles for hydrodynamic modeling, they actually make it ideal for molecular dynamics: precisely because the final system is so small, it becomes possible to perform a complete MD simulation of the collapse. In fact, sonoluminescence is somewhat unique in this regard. Usually the systems directly simulated with molecular dynamics are many orders of magnitude smaller—fewer particles, shorter time scales—than the corresponding systems realized in experiments or in nature, and this gap is too large to be eliminated by increases in computing power [15]. In contrast, the number of particles within the interior of a small SL bubble is comparable to the number of simulation particles that can be handled with current computational facilities.

For example, a typical SL bubble driven at 30 kHz has an ambient radius of 6 μm and contains 2.25×10^{10} particles. At the extreme, SL bubbles containing on the order of several million particles have been observed in systems driven at megahertz frequencies [16]. This compares well with simulations, where we have been able to compute the gas dynamics of a 10^6 particle bubble collapse using a run time of a few days on a single processor workstation-grade computer. Parallel processing simulations would make 10×10^6 to 100×10^6 particle simulations feasible. As the number of simulation particles reaches that in real systems, the remaining computer power can be used to add in more complex atomic physics, and thus allow more detailed study of the processes involved.

We note that an interesting and related molecular dynamics simulation of a (planar) piston driven shock wave in a hard sphere gas has been carried out recently in Ref. [17] and contrasted with the direct simulation Monte Carlo method. Also, since the completion of this paper [18], it has come to our attention that a molecular dynamics modeling of sonoluminescence, including multiple species, asymmetric bubbles, and chemical reaction, has also been carried out in Refs. [19,20]. In Ref. [19] the evolution of an argon gas bubble is considered. The interior of the bubble is simulated according to a molecular dynamics model. The bubble wall dynamics follows the Rayleigh-Plesset equation so that the gas and liquid dynamics are coupled by the pressure at the bubble wall. The boundary between the gas and the liquid is assumed to give energy conserving specular collisions. The authors conclude in Ref. [19] that "the MD simulations predict steep compression waves and also shock waves in collapsing bubbles as do comparable continuum approaches." A key difference between these simulations and our own is that Refs. [19,20] simulate typical (10^{10} particle) bubbles using hard sphere particles which each represent tens (or hundreds) of thousands of atoms. Particle dynamics must therefore be modeled using scaled atomic properties. However, the simulations described in this paper use the standard atomic properties (including a dependence of particle radius on relative collision speed). The bubbles studied here are therefore smaller than the "standard" SL bubbles but in fact are comparable in size to SL bubbles that form at 10 MHz [16]. Despite these fundamental differences, the temperature profiles found in Ref. [19] are in qualitative agreement with our own adiabatic argon simulations in Sec. IV C. Both predict rather sharply profiled temperatures, especially near the light emitting hot spot (in contrast with recent uniform bubble theories—see Sec. I D). Quantitatively, it is more difficult to make comparisons as the simulations in Ref. [19] do not consider ionization and so naturally obtain temperatures in excess of our own.

D. Predictive modeling goals and preliminary results

The overall goal of the MD modeling is to generate a better understanding of the processes that result in energy focusing during SL. This is to be accomplished through a dual approach of model prediction and model validation: we use the model to illustrate the phenomena that cannot be experimentally observed during the collapse, and also to make predictions that can be experimentally validated.

The basic experimental unknown in SL is the degree of energy focusing that is achieved inside of the bubble. For example, the spectral density of light from helium bubbles in water is still increasing at wavelengths as short as 200 nm (energy exceeding 6 eV), where the extinction coefficient of water cuts off the measurement [6]. Related to the question of energy focusing are the detailed questions of whether there is shock formation within the bubble, whether there is plasma formation, and what peak temperatures are achieved during the collapse. For example, the most extreme theoretical estimates suggest that the interior may reach temperatures sufficient to induce deuterium-tritium fusion [21]. Over the range of parameter space studied, shock formation and strong ionization appear to be typical, and the *lowest* peak temperatures found in our simulations are about 40 000 K, with the highest approaching 500 000 K. Our findings also indicate that boundary conditions strongly affect the interior motion. With a low, fixed temperature (i.e., heat bath) con-

dition the peak temperatures and internal gradients are higher than for adiabatic motion.

The nonintuitive effect, whereby a heat bath leads to greater energy focusing (i.e., higher peak temperatures) provides an explanation of a key experimentally established paradox. Although helium and xenon have strongly different physical properties (e.g., speed of sound and ionization potential), their measured light emission is similar [22]. In fact, the speed of sound in helium is so high as to preclude the formation of a shock wave in a collapsing bubble *in the adiabatic approximation*. The low speed of sound in xenon facilitates the formation of an imploding shock wave. When the heat bath boundary condition is imposed on the He bubble, the smooth response to adiabatic forcing is replaced by a sharply focused profile that is similar in structure to the xenon bubble.

This is an appropriate point to comment on the existing theories of sonoluminescence. All of these theories (e.g., Refs. [5,7,14]) interpret the light emission as being due to thermal bremsstrahlung from a transparent plasma. These views are confounded by the observation that SL is in many cases accurately matched by a blackbody spectrum, which implies an opaque emitter [23]. Whether extensions of the simulation to include photon-matter interactions will shed light on this key issue remains an open challenge. Another shortcoming of the weak ionization theory of SL is that Xe should emit 1000 times more strongly than He. This factor of 1000 contrasts strongly with the experimentally observed factor of about 4 [22,24]. The reason for this theoretical discrepancy is the difference in ionization potentials which leads to an exponentially suppressed response from He. It is interesting to note that our MD model with heat bath boundary conditions leads to a spiked behavior for helium containing bubbles. In this limit the peak ionization in the helium bubble is not weak but about 1/5 of that of the xenon bubble.

We also find that in the process of forming these steep profiles the gas passes through states where the mean free path is greater than the characteristic distance over which the temperature varies. See Sec. IV B. This is the regime in which the validity of the continuum approach can be doubted.

A key experimental observable in SL is the duration of the light flash, or ''flash width'' [4], because knowledge of this puts constraints on the underlying mechanism of light emission. This can be used as a validation point for any model or theory. For example, volume radiation from a plasma will yield a different flash width than surface radiation from a blackbody. Since our simulations do not include fundamental radiative mechanisms such as atomic excitation or charged particle acceleration, our current MD model cannot directly determine the light emitting mechanism or the flash width. However, a prediction about the flash width can be obtained from our calculation of the peak temperature as a function of time, assuming the light emission occurs while the peak temperature is high. See Ref. [12] for a variety of continuum calculations for the width of the temperature peak in argon bubbles. Our molecular dynamics simulations for much smaller helium bubbles show that simple adiabatic compression does not produce a sharp temperature spike in time, but the thermal boundary condition causes a spike with a duration that scales with the ambient bubble radius. This result suggests that the flash width may scale with the ambient bubble radius. If valid, this scaling suggests that at high acoustic frequencies ($\sim$10 MHz) [16] the duration of a SL flash could be about equal to or less than 1 ps.

E. Outline of the paper

The outline of the paper is as follows. Sec. II describes the model for the bubble collapse in detail. Section III outlines the principle algorithms used to evolve the hard sphere system. Section IV provides detailed results from our MD simulations. Finally, Sec. V contains a summary of our observations, and lists interesting future areas of investigation suggested by our molecular dynamics modeling of sonoluminescence.

II. MODELING SONOLUMINESCENCE BUBBLES

In this section, we present our molecular dynamics model for SL bubbles. The overall strategy is to model the system as a spherical piston that compresses a gas of hard spheres, with energy deducted from the system for ionization events at higher temperatures. The details and motivations for this are given in the following subsections.

A. Model parameters

We want to focus on the simulation of single bubble sonoluminescence, so that results can be compared to the best studied experimental SL systems. Such bubbles remain spherical during their collapse [25], and their behavior is parametrized by their ambient radius (the radius they have when at rest at the ambient pressure) and their maximum radius (the radius they attain when maximally expanded at the low pressure point of the applied sound field).

We cannot directly simulate all such SL bubbles, since they may contain several orders of magnitude more gas particles than our computational budget can accommodate. Typically, we can afford to do a calculation with some given number of simulation particles, N, and the question becomes how large of a bubble can we directly simulate. The ambient radius, R_0, is related to the number of gas particles, N, by the ideal gas equation of state

$$P_0\left(\frac{4}{3}\pi R_0^3\right) = kT_0N,$$

where $T_0 = 300$ K and $P_0 = 1$ atm are the ambient temperature and the pressure, and k is the Boltzmann's constant. Thus we see that the fewer the simulation particles we use, the smaller the ambient size of the bubble being simulated.

Once the ambient size is determined by our simulation budget, we are free to choose any maximum radius. For experimentally relevant simulations, the maximum radius R_m is chosen to yield the same ratio of R_m/R_0 [$\sim$10] for the MD simulation as is seen in experimental SL bubbles. This is natural because this ratio is a measure of the available energy stored in the expansion, since the stored energy/particle due

to the work done by expanding to the maximum volume V_m against the applied pressure P_0 is

$$\frac{P_0 V_m}{N} = kT_0 \frac{R_m^3}{R_0^3}.$$

B. Bubble collapse

Since the bubble remains spherical during collapse, its boundary dynamics are described entirely by the radius as a function of time, $R(t)$. We are concerned with energy focusing processes and gas dynamics inside the bubble, and in this spirit we will take $R(t)$ as being known. A convenient model of the spherical piston that captures some qualitative features of the supersonic collapse is provided by Rayleigh's equation [5]

$$R\ddot{R} + \frac{3}{2}\dot{R}^2 = [P_g(R) - P_0]/\rho, \tag{1}$$

with a van der Waals hard core equation of state

$$P_g(R) = \frac{P_0 R_0^{3\gamma}}{(R^3 - a^3)^\gamma}, \tag{2}$$

$\gamma = 5/3$, where a is the radius of the gas in the bubble when compressed to its van der Waals hard core ($R_0/a = 10.1$, 9.15, 7.84 for He, Ar, Xe), ρ is the density of the surrounding fluid, and the initial condition for the solution to Eq. (1) is that $\dot{R} = 0$ when $R = R_m$. We emphasize that the derivation of Eqs. (1) and (2) applies only for small Mach number motion and thus they are invalid as a fundamental theory for SL [22]. However, in our initial attempt to simulate SL with molecular dynamics, we are interested in possible focusing processes within the bubble and use of Eqs. (1) and (2) as a launch condition appears appropriate since the resulting $R(t)$ reasonably approximates the gross bubble pulsation [5].

Consistent with this approximation, viscous damping and acoustic radiation have also been neglected. At the next level of simulation one should include a self-consistently determined boundary condition on pressure at the bubble's wall. In this way, energy loss due to acoustic radiation is properly accounted for.

As a point of comparison, it is worth noting that the adiabatic equations of state for the van der Waals pressure $P_g(\cdot)$ and the computed *equilibrium* hard sphere pressure $P_{hs}(\cdot)$ (the equilibrium pressure as a function of radius as the radius is decreased *slowly* on the hard spheres with no heat conduction) agree very well, except at bubble radii near the hard core, as plotted in Fig. 1 for helium (with the other noble gases also in good agreement, except near the hard core). At small radii, the van der Waals pressure diverges as R tends to a and the $P_{hs}(\cdot)$ diverges as R tends to

$$a_{hs} \equiv \left(\frac{N}{0.63}\right)^{1/3} \frac{\sigma}{2},$$

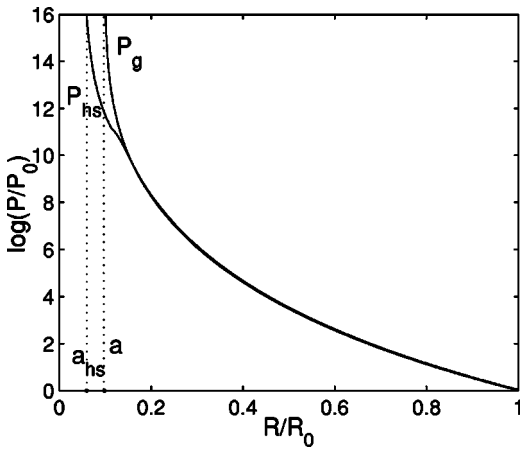

FIG. 1. Plots of the adiabatic equations of state for the van der Waals pressure P_g and the computed hard sphere pressure P_{hs} for helium, using the natural logarithm.

which is the minimum radius for random closed packing [26].

C. Gas dynamics

It has been observed that for SL in water, the bubble must contain sufficient amount of a noble gas. Thus in many single bubble SL experiments, the water is first degassed to remove atmospheric gases, and then resaturated with a noble gas to produce pure noble gas bubbles. We will focus our gas dynamic model on this system, since it is a frequent experimental model and also because it allows the simplest molecular gas dynamics models. Because the gas is noble, it consists of isolated atoms that do not engage in chemical reactions. Thus we can model it with simple gas particles that have no rotational or internal vibrational degrees of freedom, and which do not engage in any chemical reactions with the water walls of the bubble, even at elevated temperatures.

Molecular dynamics simulations for such simple gas particles fall into two broad categories, defined by the way they treat interatomic forces. The forces can either be given by a potential that varies continuously with radius from the atom center (''soft sphere''), or by a potential that is a step function of radius (''hard sphere''). The latter particles behave simply like billiard balls. While the continuous potential are more physically realistic, they are also much more costly to compute with. This is because numerical time integration methods must be used to compute the particle motions in response to the continuously varying forces, and the time step must be small enough to accurately resolve all particle trajectories in the system. Thus the motion of a few fast moving particles will force the use of a small, costly time step for all particles in the system. In contrast, step potentials do not experience this problem because they evolve in time by a series of discrete collision events. No explicit numerical integration is needed since impulsive collisions are carried out only when atoms interact, and between collisions each atom follows an independent linear trajectory. Thus each atom effectively uses its own optimally large time step, in-

stead of an excessively small step imposed by the the fastest particles in the system. Moreover, there is no numerical integration error because trajectories are evaluated to within the roundoff error of the machine [15].

Because of this difference in computational cost, it is desirable to use the hard sphere model if it can capture the physics of interest. In our case, we want to get accurate gas dynamics at mid to high energies for fairly large numbers of particles. Whether hard spheres are sufficient to model this regime in an SL bubble is an empirical question, but such models have been shown to yield accurate predictions of noble gas viscosity from room temperature up to the gas ionization temperatures [27]. We take this to be a reasonable validation that a hard sphere gas provides a good model for the gas dynamics encountered during bubble collapse, at least up to ionization temperatures. Near that point and beyond, it also seems reasonable that a hard sphere model applies, since the softer parts of the potential are all the more insignificant for high-energy collisions.

The dynamics of a hard sphere system involve processing impulsive collisions at the collision times. To illustrate, consider two particles separated by a relative position $\mathbf{r}$ and having a relative velocity $\mathbf{v}$. These particles collide if their separation equals the atomic diameter σ at some time τ in the future. If such a collision occurs, then τ is the smaller positive solution of

$$|\mathbf{r}+\mathbf{v}\tau| = \sigma,$$

which has a solution

$$\tau = -\frac{1}{\mathbf{v}\cdot\mathbf{v}}[\mathbf{r}\cdot\mathbf{v} + \sqrt{(\mathbf{r}\cdot\mathbf{v})^2 - \mathbf{v}\cdot\mathbf{v}(\mathbf{r}\cdot\mathbf{r}-\sigma^2)}].$$

Collisions are carried out impulsively so that the change in velocities preserves energy and momentum. Specifically,

$$\Delta\mathbf{v}_1 = -\Delta\mathbf{v}_2 = -\frac{(\mathbf{r}_c\cdot\mathbf{v})\mathbf{r}_c}{\sigma^2},$$

where $\Delta\mathbf{v}_1$ is the change in velocity of the first particle, $\Delta\mathbf{v}_2$ is the change in velocity of the second particle, and $\mathbf{r}_c$ is the relative position at the time of collision.

Extensions to step potentials that consist of a hard repulsive core surrounded by an attractive well are also possible, see Ref. [15] for details.

D. Bubble wall boundary conditions

When a gas particle hits the bubble wall, it might simply be directed back into the interior by a strong collision with a liquid molecule, or it may penetrate into the liquid, undergoing multiple thermalizing collisions. In the latter case, assuming the liquid is already saturated with gas atoms, the thermalized atom (or an equivalent one from the saturated liquid reservoir) will ultimately random walk its way back into the bubble interior.

For our MD model, we will idealize these two modes of boundary interaction either as energy conserving *specular* collisions or as *heat bath* boundary conditions.

For the case of specular collisions, particles reflect from the boundary with a speed equal to the collision speed in the local rest frame of the wall. The direction of propagation is determined according to the law of reflection, where the angle of incidence equals the angle of reflection with respect to the local normal to the bubble surface.

For heat bath boundary conditions, when a particle hits the boundary it is assigned a thermal velocity at the ambient liquid temperature T_0, and the direction of propagation back into the interior is chosen according to a suitable angular distribution. We ignore the small time lag that might exist between exit and reentry for the thermalized gas particle.

For the angular distribution, we use the *cosine distribution*, where the angle of reflection θ is assigned randomly according to a probability density function,

$$f(\theta) = \begin{cases} (1/2)\cos\theta & \text{for} \quad -\pi/2 \leqslant \theta \leqslant \pi/2, \\ 0 & \text{otherwise.} \end{cases}$$

We have also tried a uniform distribution in angle in selected test cases. This did not significantly change the simulation results. (Nonetheless, we note that there may exist situations where results differ qualitatively since a uniform distribution has a greater tendency to cause reflected particles to build up near the wall.)

In reality, we expect that the physical boundary will have some characteristics of both models. By investigating these extreme cases[1] we hope to see the full range of effects that boundary conditions can have on the bubble dynamics.

E. Initialization

Initially the bubble is at its maximum radius, $(R=R_m)$, and particles are moving in uniformly distributed random directions, with the same thermal speed $v_{th}(T_i)=\sqrt{3T_i k/m}$, where T_i is the initial temperature and m is the mass of the particle. Randomization of speeds is not necessary, since the particles rapidly thermalize their energies in any case.

As mentioned above, the MD simulation will be applied separately to heat bath and specular reflection boundary conditions. Emphasis is placed on the motion for those times when the radius is less than its ambient value. This is the interesting, or fast, portion of the cycle where use of molecular dynamics is indicated. Since motion for radii larger than ambient is slow, thermal conduction to the surrounding fluid will lead to a constant temperature during this part of the cycle [28] and it is therefore appropriate to require that temperature agrees with its ambient value when R passes through its ambient value.

For calculations that begin at the maximum radius, this fact is automatically included in calculations that employ heat bath boundary conditions. The specular condition, however, generates unphysically large temperatures when the bubble collapses to its ambient size, due to adiabatic heating.

[1]They are extreme in the sense that specular collisions do not transfer any thermal energy out of the bubble, while heat bath conditions give the maximal thermal energy transfer.

TABLE I. Hard sphere diameters and masses.

Gas	Mass (g/mol)	Diameter (Å)
He	4.00	2.18
Ar	39.95	3.66
Xe	131.29	4.92

TABLE II. VSS molecular parameters.

Gas	ω	μ_{ref} (N s m^{-2})	α
He	0.67	1.865×10^{-5}	1.26
Ar	0.81	2.117×10^{-5}	1.40
Xe	0.85	2.107×10^{-5}	1.44

In order to achieve the ambient temperature T_0 at the ambient radius R_0, the initial temperature must be scaled down to $T_i = T_0/(R_m/R_0)^2 = T_0/100$. The factor of $(R_0/R_m)^2$ approximately cancels the adiabatic heating (since $TR^2 = \text{const}$ in a $\gamma = 5/3$ ideal gas at constant entropy) during the initial, slow portion of the collapse. Note that this scaling can be viewed as a simple way to roughly account for the heat transfer from the gas into the liquid during the slow portion of the collapse. Another alternative would be to use heat bath boundary conditions during the slow part of the collapse. While we have not examined this possibility in detail, we have found that when applied to helium bubbles this alternative gives ambient temperature profiles that are within 20% of our adiabatic model.

F. Hard sphere properties

The basic properties associated with the hard sphere model are the gas particle mass and diameter. The mass is simply taken to be the mass of the noble gas atom being simulated, see Table I. The choice of a proper hard sphere diameter is a much more difficult question. The diameter should represent the statistical average distance of approach of the particles during collisions, and thus in general it should depend on the collision energy.

In our most basic model we will neglect this temperature dependence and choose particle diameters that have been derived from the kinetic theory for the viscosity of a gas at room temperature [29–31]. To produce a more realistic model for higher temperature regimes of interest in SL, the hard sphere diameter should depend on the relative velocity of the colliding particles. A variety of models have been proposed to take this effect into account [27]. These include the variable hard sphere (VHS) model [32], the variable soft sphere (VSS) model [33,34], and the generalized hard sphere (GHS) model [35], which is an extension of the VHS and VSS models. In this paper, we are mainly interested in contrasting how variable and constant hard sphere diameters affect our simulations, so the recent VSS model is chosen for its combination of simplicity and calibrated accuracy. In fact, we find that the VSS model and constant diameter models often produce quantitatively similar results, see Sec. IV for details.

The viscosity based diameter of a VSS particle is

$$\sigma = \left(\frac{5(\alpha+1)(\alpha+2)(m/\pi)^{1/2}(kT_{ref})^{\omega}}{16\alpha\Gamma(9/2-\omega)\mu_{ref}E_t^{\omega-1/2}} \right)^{1/2}, \qquad (3)$$

where k is the Boltzmann's constant, m is the mass of the particle, ω is the dimensionless viscosity index, and α is a dimensionless constant for each gas. The constant μ_{ref} represents the viscosity at the reference temperature ($T_{ref} = 273$ K) and pressure (1 atm). Finally, $E_t = (1/2)m_r c_r^2$ is the asymptotic kinetic energy where m_r is the reduced mass,

$$m_r = \frac{m_{particle_1} m_{particle_2}}{m_{particle_1} + m_{particle_2}},$$

and c_r is the relative velocity between the particles. Tabulated values for these new parameters are provided in Refs. [27,36] and are summarized in Table II.

G. Ionization Effects

Near the minimum radius of the bubble, collisions may become sufficiently energetic to ionize the gas atoms. Ionization exerts a very strong cooling effect on the gas, since on the order of 10 eV of thermal energy is removed from the gas by each ionization event. Indeed, if such energy losses are not included, xenon simulations can reach temperatures in excess of 10^6 K, while the inclusion of ionization cooling brings these peak temperatures down substantially (see Sec. IV). This clearly shows that some degree of ionization must occur during collapse, and that its cooling effects must be included for proper prediction of peak temperatures. The ions and free electrons produced by ionization will move according to Coulomb forces, but the need to incorporate these effects is not as clear, and their inclusion is more difficult and expensive due to the long range effects, so they will not be included in this first treatment. We will only consider the impact of ionization on energy accounting.

For the purpose of energy accounting, an ionization ultimately produces two losses: the energy of ionization is lost immediately, and the emitted cold electron will quickly be heated to thermal equilibrium with the gas through subsequent electron-gas collisions, thus extracting an additional one particle's worth of thermal energy by the equipartition of energy.

For our model, whenever the collision energy exceeds the ionization potential we will simply assume that ionization occurs with a probability of 1 and we deduct a suitable amount of energy from the pair. We also keep track of how many electrons each particle has lost, so that we can make use of the appropriate next ionization energies and calculate the local ionization levels. The direction of gas particle propagation is updated exactly as without ionization, see Sec. II C for details.

More precisely, if the kinetic energy (in the center of mass frame) of two colliding particles is greater than the next ionization energy of either of the pair (which may already be ionized), that particle loses an additional electron. We ac-

TABLE III. Ionization potential (MJ/mol). Each entry represents the energy required to ionize the indicated state.

Gas	Ion							
	Neutral	1+	2+	3+	4+	5+	6+	7+
He [37]	2.37	5.25						
Ar [37]	1.52	2.67	3.93	5.77	7.24	8.78	12.0	13.8
Xe [37,38]	1.17	2.05	3.10	4.60	5.76	6.93	9.46	10.8

count for the net energy loss by setting the kinetic energy of the pair to be

$$\frac{2}{3}\left(E_0-\chi\frac{E_0}{E}\right),$$

where E_0 is the original kinetic energy of the particle, E is the kinetic energy of both particles before the collision, and χ is the ionization potential of the minimally charged particle.

Note that the final kinetic energy of the pair is the initial energy, minus the ionization energy, with an additional 1/3 deducted to represent the subsequent energy lost to thermalizing the electron. This is not the only possible way to include this effect, and of course in reality this process involves losses from other gas particles besides the colliding pair, but this approach is the simplest way to include the effect.

We also do not account for subsequent electron-ion recombination to neutral atoms, although this would be interesting to include at the next level of description. In particular, this could be an interesting source of radiation as the hot spot decays.

For reference, the approximate ionization potentials used for the three noble gases are provided in Table III.

III. ALGORITHM

Efficient algorithms are needed to evolve our hard sphere model for sonoluminescence since a naive coding is prohibitively slow for anything more than a few thousand particles. To achieve this goal, we modify and extend existing methods [15] rather than develop new algorithms and codes from scratch. This section outlines the principal algorithms used to evolve our hard sphere system. Further details and basic codes are provided in Ref. [15].

A. Cell subdivision

The hard sphere simulation proceeds according to a time ordered sequence of collision events [15,39]. But clearly a direct determination of the next event for a given particle is impractical in our large simulations because $O(N)$ work is required *per particle* to examine all possible collision partners, where N is the total number of particles.

Fortunately, this work can be reduced to a constant independent of N by dividing the bubble into a number of cells [15,39]. Since we want a relatively small number of particles in each cell *and* we want the number of cells to be comparable to the number of particles in the simulation, the size of the cells must be reduced as the bubble collapses. We use a straightforward subdivision procedure to accomplish this task. Initially, the bubble is subdivided into approximately $8N$ square, identical cells. Every time the bubble declines by a factor of two in diameter, cell size is reduced by a factor of two (keeping in mind that we must stop the procedure once the cell diameters reach the particle diameter). Note that we do not need to recompute which particle belongs to which cell after each collision. Instead, we introduce a cell crossing event and update a particle's cell location only when the corresponding cell crossing event is processed (cf. Ref. [15,39]).

B. Event calendar

Because we require information on when particle collisions, hard wall collisions, and cell crossings occur, some sort of *event calendar* is needed. This calendar will store many future events. As collisions and cell crossings occur, newly predicted collisions and cell crossings must be added to the calendar and events that are no longer relevant must be removed [15].

Of course, it is essential that the calendar can be managed efficiently both in terms of memory and CPU usage. To meet this requirement, we utilize the binary tree data structure described in Refs. [15,40]. It is interesting that estimates of the theoretical performance of the tree structure are possible in a number of instances [41,15]. For example, if a tree is constructed from a series of events that are randomly distributed, the average number of nodal tests to insert a new node into the tree is $2 \ln N$. Also, the average number of cycles to delete a randomly selected node is a constant independent of N. It is worth noting that measurements have been performed to confirm these results in actual MD simulations [40]. Our sonoluminescence simulations spend most of the CPU time on compressing the bubble from its maximum radius to the ambient radius. Since the bubble is fairly uniform in this regime, the assumption of a random distribution of events seems plausible and we expect that this type of estimate on theoretical performance should hold. (However, near the short-lived hot spot the behavior is far from equilibrium and this assumption on randomness may be invalid.) A detailed study of the theoretical performance of the tree structure will be the focus of subsequent work.

C. Average properties

We need to evaluate spatially dependent average properties of the gas at various times. To minimize statistical fluctuations, we assume that the results are radially symmetric and average over shells that are (1/40)th of the bubble radius. We calculate dimensionless values for density, temperature, velocity, and average charge as follows.

(1) The dimensionless density is given by the density divided by the average ambient density.

(2) The dimensionless velocity is given by the velocity divided by the ambient speed of sound $\sqrt{\gamma k T_0/m}$, where γ is the ratio of heat capacities and m is the mass of a single particle.

(3) The dimensionless temperature is given by the temperature divided by the ambient temperature, T_0. Specifically,

$$T=\frac{m}{3NkT_0}\sum_{i}^{N}(v_i^2-v_n^2),$$

where the summation is over all N particles in the shell, v_i is the speed of the ith particle, and v_n is the normal speed of the gas in the shell.

(4) Ionization is simply the average charge per particle.

(5) In each case we plot properties as a function of a dimensionless bubble radius, r, which equals the physical radius $R(t)$ divided by a constant approximating the atomic diameter. For helium, this constant is chosen to be 2.18 Å (see Table I). For argon and xenon these constants are chosen to be 4.11 Å and 5.65 Å, respectively. (These latter two choices represent average VSS model values at 273 K and also approximate the values given in Table I.)

See Ref. [15] for further details on calculating equilibrium and transport properties for hard sphere models.

IV. SIMULATION RESULTS

In this section we simulate the collapse of a sonoluminescing bubble from its maximum radius to its hot spot. Our focus is on how boundary conditions affect the interior dynamics of the collapse. Results for helium, argon, and xenon are presented.

The section begins with a study of the collapse of 10^6 particle bubbles and concludes by addressing how simulations vary according to ambient bubble size.

A. Helium bubbles with specular BCs

We first consider evolving a bubble of 10^6 Helium atoms using specular boundary conditions.

With the *constant diameter model* and *no ionization* the temperature and density increase uniformly as the bubble collapses to the minimum radius. After the minimum radius is attained, the temperature increases towards the center of the bubble and decreases at the expanding outer boundary of the bubble, with a peak temperature of about 80 000 K reached at the center. (At these temperatures, it is clear that ionization events will occur; so the remainder of our simulations consider ionization.) See Fig. 2 for plots of the density, temperature, and velocity as a function of distance from the center of the bubble at various bubble radii.

With the *constant diameter model* and *ionization* we again find that the temperature and density increase uniformly as the bubble collapses to the minimum radius. However, after the minimum radius is attained, ionization causes the temperature to decrease across the entire bubble rather than just at the boundary of the bubble (although cooling occurs most rapidly at the bubble boundary). A peak temperature of about 40 000 K is attained at the minimum radius. It is particularly worth noting that recorded properties are nearly constant throughout the bubble when the peak temperature occurs—see Fig. 3.

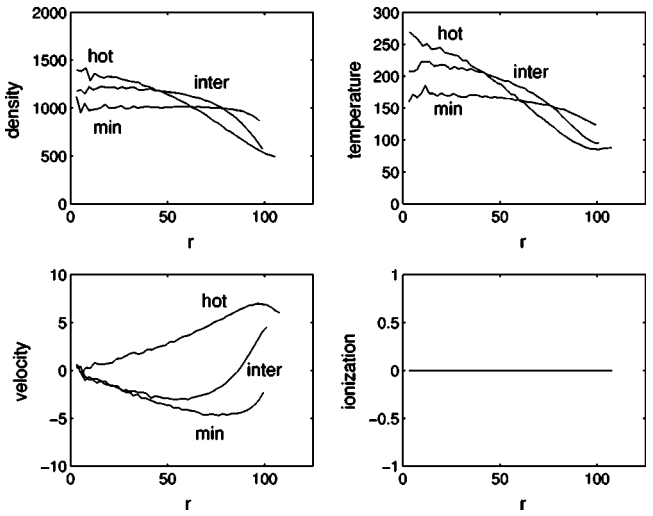

FIG. 2. The helium bubble with specular BCs, constant diameter particles, and no ionization. ''min'' gives properties at the minimum radius $R_{min}=99.4$. ''hot'' gives properties at the peak temperature. In this simulation, the peak temperature occurs soon after the minimum radius is attained and corresponds to a radius of 107.7. ''inter'' gives properties at an intermediate time. Here $R_{inter}=101.0$.

Changing to the VSS *diameter model* gives very similar results, except now ionization occurs less frequently because the effective size of the particles is smaller. Because less ionization occurs, the temperature continues to increase for a short while after the minimum bubble radius is attained, leading to a peak temperature of about 45 000 K, see Fig. 4 for details.

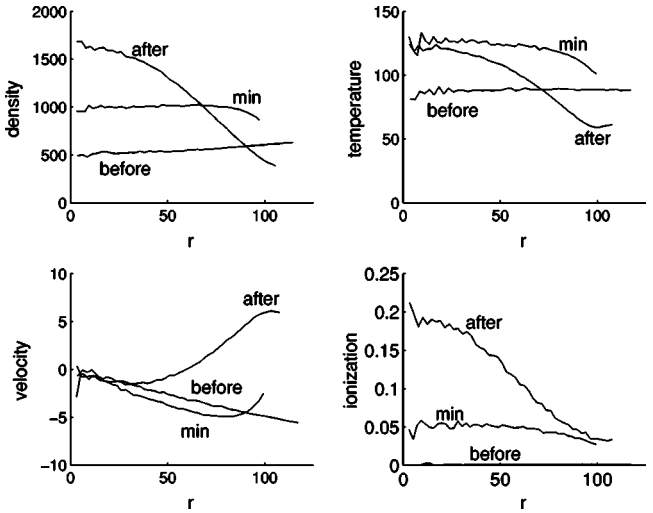

FIG. 3. The helium bubble with specular BCs, constant diameter particles, and ionization. ''min'' gives properties at the minimum radius $R_{min}=99.4$. ''before'' and ''after'' give properties at times before and after the minimum radius is attained. In this simulation, ''before'' and ''after'' correspond to radii of 117.2 and 107.7, respectively. We also note that the peak temperature approximately coincides with the minimum radius in this example.

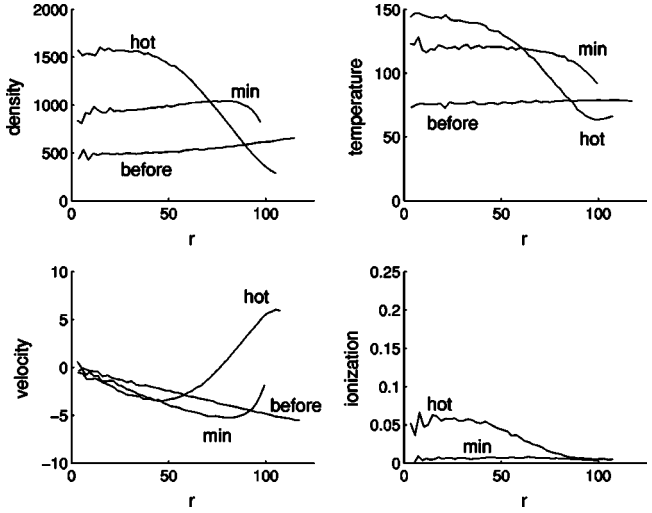

FIG. 4. The helium bubble with specular BCs, VSS diameter particles, and ionization. ''min'' gives properties at the minimum radius $R_{min}=99.4$. ''hot'' gives properties at the peak temperature. In this simulation, the peak temperature occurs after the minimum radius is attained and corresponds to a radius of 107.5. ''before'' gives properties before the minimum radius is attained. Here, $R_{before}=117.4$.

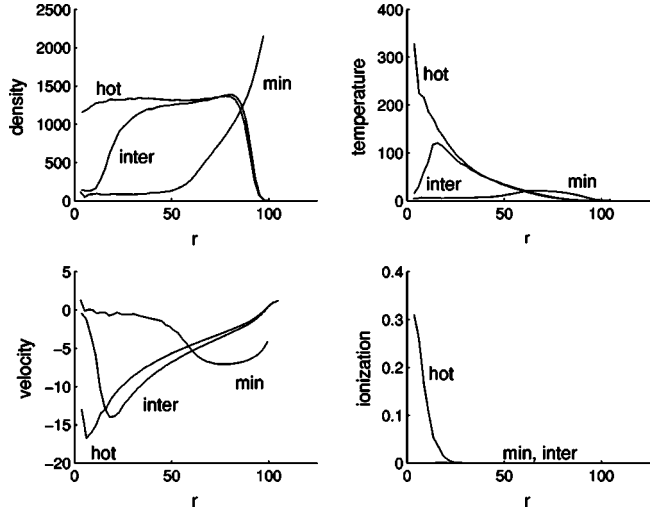

FIG. 5. The helium bubble with heat bath BCs, constant diameter particles, and ionization. ''min'' gives properties at the minimum radius $R_{min}=99.4$. ''hot'' gives properties at the peak temperature. In this simulation, the peak temperature occurs soon after the minimum radius is attained and corresponds to a radius of 117.2. ''inter'' gives properties at an intermediate time. Here $R_{inter}=114.8$.

B. Helium bubbles with heat bath BCs

Our next set of simulations evolve a bubble of 10^6 Helium atoms using heat bath boundary conditions (BCs) and ionization.

With the *constant diameter model* the density increases dramatically at the edge of the bubble as the minimum radius is attained. Temperature and velocity are also much more profiled than for specular boundary conditions, with peaks occurring about 25% of the way from the boundary of the bubble to the center. No ionization has occurred at the minimum radius. For a short time after the minimum radius is attained,[2] the peak temperature of the bubble continues to increase (to a maximum of 95 000 K), and temperature and density profiles become even more pronounced—see Fig. 5. At first sight, it is counterintuitive that heat bath boundaries create conditions whereby the cooling from the boundary leads to greater energy focusing and higher peak temperatures. Perhaps cooling lowers the speed of sound and enhances the nonlinear response to the high speed $\dot{R}$ of collapse.

It is particularly interesting that in the process of forming these steep profiles the gas passes through states where the mean free path is greater than the characteristic distance over which the temperature varies, see Fig. 6. This is the regime in which the validity of the continuum approach can be doubted.

Changing to the VSS *diameter model* gives very similar results, except now ionization occurs less frequently because the effective size of the particles is smaller, see Fig. 7 for details.

C. Argon and xenon bubbles with specular BCs

Our next set of simulations evolve 10^6 particle argon and xenon bubbles using specular boundary conditions and ionization.

We start by considering an argon bubble with the VSS *diameter model*. Because the speed of sound is slower in argon than in helium we expect argon simulations to exhibit much sharper profiles than helium. This is indeed the case. Moreover, our simulation results are surprisingly similar to those for helium with *heat bath boundaries*. Density increases at the edge of the bubble as the minimum radius is attained. Temperature and velocity are sharply profiled, with

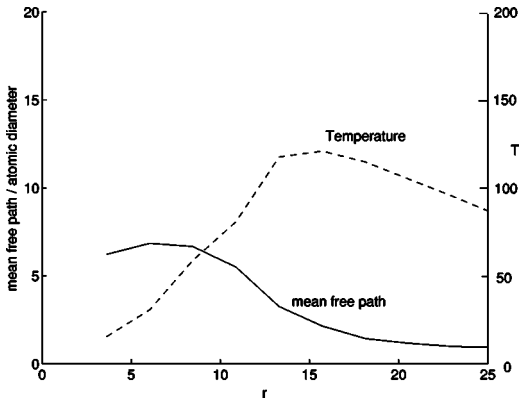

FIG. 6. A plot of mean free path/atomic diameter (solid line) and temperature (dashed line) at $R_{inter}=114.8$ for the helium bubble with heat bath BCs, constant diameter particles, and ionization.

[2]Note that a vacuum forms at the bubble wall after the minimum radius is attained. This is simply an artifact of using Eq. (1) as the forcing equation for $R(t)$.

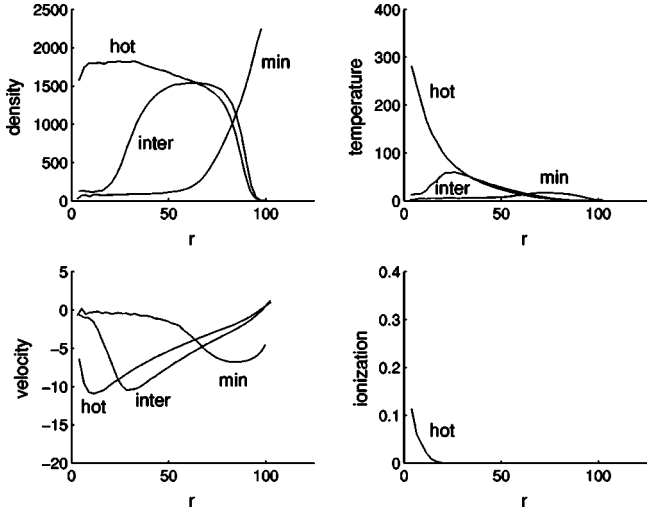

FIG. 7. The helium bubble with heat bath BCs, VSS diameter particles, and ionization. ''min'' gives properties at the minimum radius $R_{min}=99.4$. ''hot'' gives properties at the peak temperature. In this simulation, the peak temperature occurs after the minimum radius is attained and corresponds to a radius of 123. ''inter'' gives properties at an intermediate time. Here $R_{inter}=117.2$.

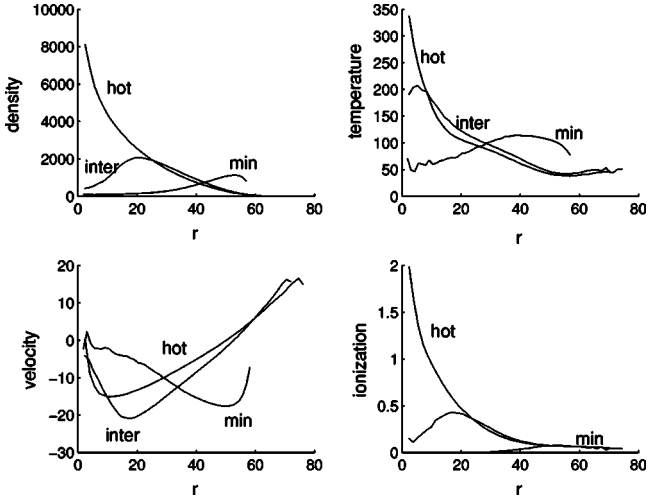

FIG. 8. The argon bubble with specular BCs, VSS diameter particles, and ionization. ''min'' gives properties at the minimum radius $R_{min}=58.2$. ''hot'' gives properties at the peak temperature. In this simulation, the peak temperature occurs after the minimum radius is attained and corresponds to a radius of 76.2. ''inter'' gives properties at an intermediate time. Here $R_{inter}=72.0$.

peaks occurring closer to the boundary of the bubble than to its center. Also, for a short time after the minimum radius is attained, the peak temperature of the bubble continues to increase rapidly (to a maximum of 100 000 K), and temperature and density profiles become even more pronounced—see Fig. 8.

Constant diameter hard sphere simulations of argon are also possible. These simulations are unique[3] in that the hot spot occurs before the minimum radius value of 58.2—see Fig. 9. As expected, this simulation gives sharper profiles than the corresponding model for helium. However, since the minimum radius is close to the minimum radius allowed by the packing of the hard spheres, the results are much more uniform than those derived using the VSS model for argon. Also note that as a result of the collapse of the bubble, energy stored at the maximum radius is converted into heating, ionization, and kinetic energy of the local center of mass. From Fig. 9 one can estimate these quantities. The average temperature of the atoms is 30 000 K, which is a thermal energy of about 3.75 eV/atom. As half the atoms are ionized, the ionization energy is about 8 eV/atom. Since electrons have about the same thermal energy as the ions, their energy is about 2 eV/atom. Taken together, these channels add to about 21 eV/atom, which is less than the 25 eV/atom available in the initial state but the difference is within the accuracy of the energy estimates. For helium at the hot spot, the energy of the hard sphere (plus ionization) is substantially less than the energy stored at R_m. This can be attributed to the fact that $a_{hs}/a \approx 0.60$. For argon, almost all the stored energy ends up in the hard sphere gas since a_{hs} is much closer to a; $a_{hs}/a \approx 0.91$. In all cases, the inclusion of a self-consistent boundary condition for the pressure will account for energy losses (e.g., radiation damping) that are only approximated by the model of Rayleigh's equation that was employed here. In those cases where strong energy focusing occurs in the interior of the collapsing bubble, the effects of a more precise boundary condition on the pressure will most likely be small. For (almost) uniform interiors (e.g., He with specular conditions) the effects of the self-consistent pressure could yield substantial corrections to the acoustic radiation damping. As we have seen, the more

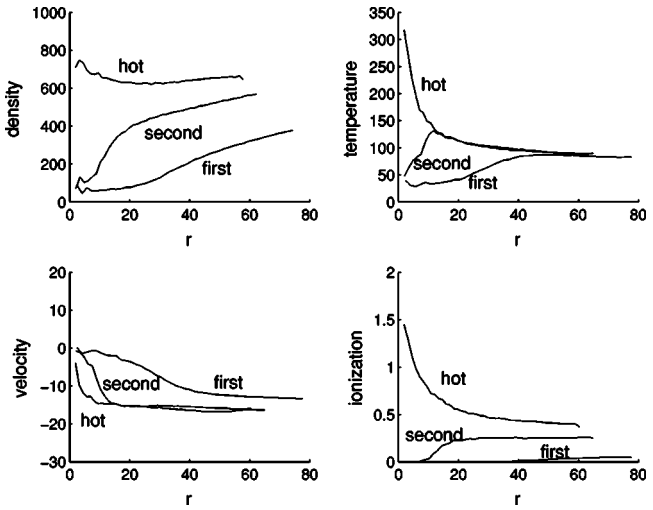

FIG. 9. The argon bubble with specular BCs, constant diameter particles, and ionization. ''hot'' gives properties at the peak temperature. In this simulation, the peak temperature occurs just before the minimum radius (of 58.2) is attained and corresponds to a radius of 60.3. ''first'' and ''second'' give properties before the peak temperature is attained. Here, $R_{first}=77.6$ and $R_{second}=64.9$.

[3]This behavior may be related to the consistency of the minimum bubble radius and the hard sphere radius. See the case of xenon below.

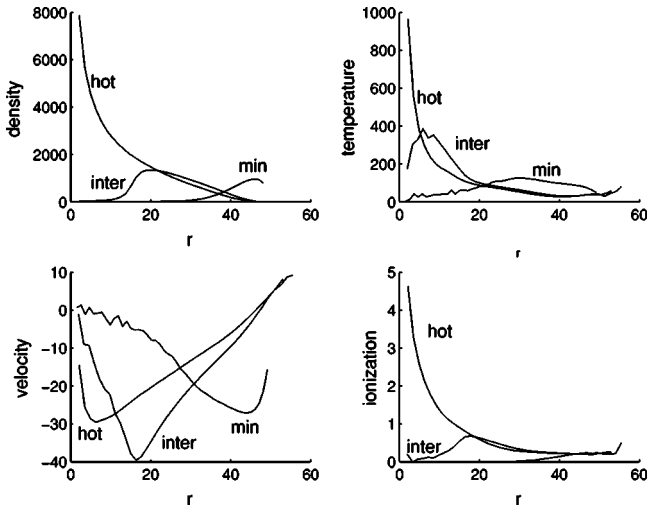

FIG. 10. The xenon bubble with specular BCs, VSS diameter particles, and ionization. ''min'' gives properties at the minimum radius $R_{min}=49.2$. ''hot'' gives properties at the peak temperature. In this simulation, the peak temperature occurs after the minimum radius is attained and corresponds to a radius of 66.7. ''inter'' gives properties at an intermediate time. Here $R_{inter}=62.2$.

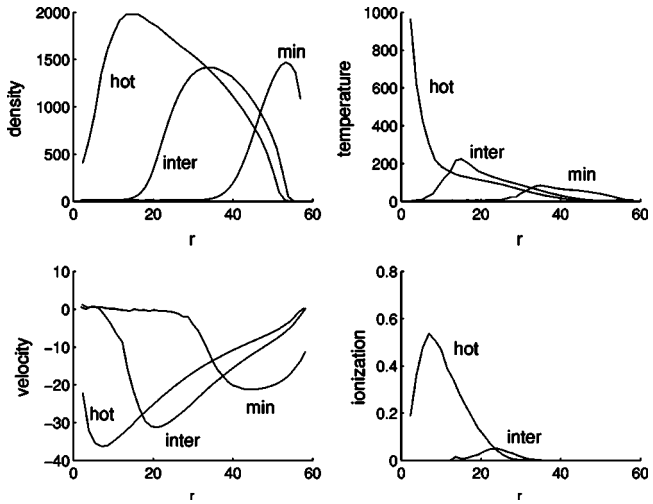

FIG. 11. The argon bubble with heat bath BCs, VSS diameter particles, and ionization. ''min'' gives properties at the minimum radius $R_{min}=58.2$. ''hot'' gives properties at the peak temperature. In this simulation, the peak temperature occurs after the minimum radius is attained and corresponds to a radius of 73.2. ''inter'' gives properties at an intermediate time. Here $R_{inter}=68.1$.

physical heat bath boundary conditions lead to energy focused states (even for He) and so the need to introduce the self-consistent pressure is not mandated by the physical comparisons to sonoluminescence considered here.

Simulations for xenon bubbles with the VSS *diameter model* were also carried out. Because the speed of sound is slower in xenon than in argon, we expect xenon simulations to exhibit even sharper profiles than argon. Indeed, this is the case and temperatures of up to 300 000 K were obtained despite the occurrence of multiple ionization (exceeding 4 per particle at the center)—see Fig. 10.

A proviso for the xenon data is that these calculations bog down before the minimum radius is attained when the constant diameter model is used, whereas the helium data are hardly affected by this modification. The explanation lies in the consistency of the minimum bubble radius ($\sim a$) and the hard sphere radius for xenon. Specifically, the minimum radius of the bubble wall is less than the minimum radius allowed by the packing of hard spheres. However, xenon simulations carried out using the VSS model are relatively insensitive to changes in a. For example, increasing a by 30% changes the peak temperature by about 35%, and leaves the qualitative features invariant. Note that in this case, $a_{hs}<a$ as with helium simulations.

D. Argon and xenon bubbles with heat bath BCs

We now consider the evolution of 10^6 particle argon and xenon bubbles using heat bath boundary conditions and ionization.

Applying the VSS *diameter model* to an argon bubble gives results that have the same qualitative features as the corresponding helium simulation, except that all properties are much more sharply profiled. Indeed, temperatures of up to 300 000 K were obtained in this simulation showing (once again) that heat bath boundaries create conditions whereby the cooling from the boundary leads to greater energy focusing and higher peak temperatures than specular boundary conditions, see Fig. 11 for details.

Simulations for xenon bubbles with the VSS *diameter model* were also carried out. Because the speed of sound is slower in xenon than in argon, xenon simulations exhibit even sharper profiles than argon. Indeed, temperatures of up to 500 000 K were obtained, see Fig. 12 for details.

As discussed in the preceding section, the constant diameter model for xenon is not able to compute down to the minimum radius since that radius is smaller than the mini-

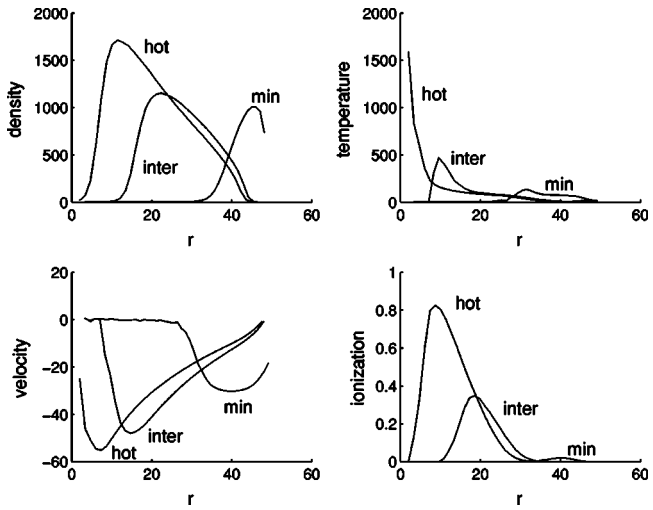

FIG. 12. The xenon bubble with heat bath BCs, VSS diameter particles, and ionization. ''min'' gives properties at the minimum radius $R_{min}=49.2$. ''hot'' gives properties at the peak temperature. In this simulation, the peak temperature occurs after the minimum radius is attained and corresponds to a radius of 60.8. ''inter'' gives properties at an intermediate time. Here $R_{inter}=63.7$.

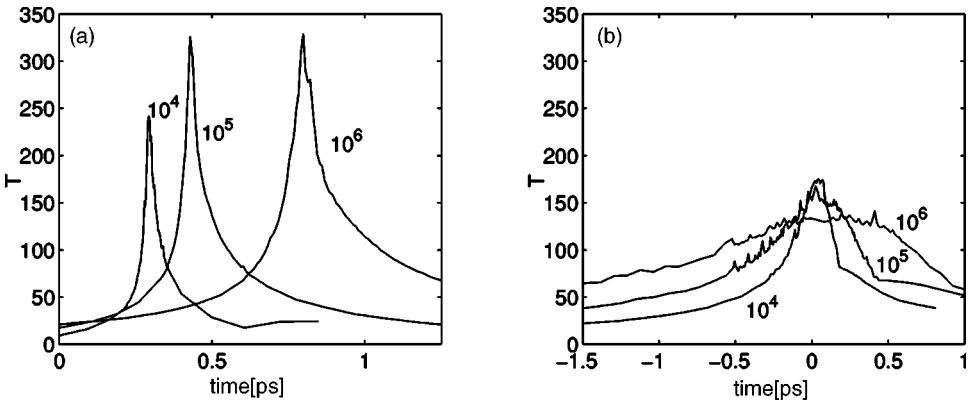

FIG. 13. Helium peak bubble temperature vs time with time = 0 marking the time corresponding to the minimum radius. (a) Heat bath boundary conditions. (b) Specular boundary conditions.

mum packing radius of the hard sphere gas. However, argon calculations are possible. These simulations are qualitatively similar to the constant diameter model for helium, but produce a more highly ionized gas (reaching an average charge of $+6$ per particle near the center) and much higher temperatures (up to 1.5×10^6 K) than any other simulations that were considered. Because such extreme values arise, it seems likely that the constant diameter model for argon also experiences a significant consistency problem near the minimum radius.

E. Flash widths

An important experimental measurement for SL bubbles is the flash width, i.e., the duration of the light emission, because this constrains the possible light emission mechanisms and thus provides a point of validation for any proposed model or theory. Since our simulations do not include the fundamental atomic excitation or charge acceleration effects responsible for radiation, the current model does not directly yield a flash width.

However, an estimated flash width can be obtained from the computed temperature as a function of time. If we assume that whatever process is responsible for the light emission is strongly dependent on the current temperature, and that it does not appreciably alter the gross gas dynamics, the flash width at a particular color is simply the length of time which the temperature exceeds the appropriate turn-on threshold. In this case, the peak temperature as a function of time is our key diagnostic quantity.

Our simulations (Fig. 13) show that emission from an adiabatic compression lacks a strong, sharp temperate spike in time, and thus the associated flash from this model would be longer and would comprise lower energy photons. In contrast, the heat bath boundary conditions yield sharp transient spike in temperature, and thus this model predicts a much shorter flash which comprises higher energy photons. In both cases it appears that the width of the spike roughly doubles as the number of particles in the bubble increases by factors of 10, from $N=10^4$ to $N=10^6$. Since each factor of 8 in particle number corresponds to a doubling of the ambient bubble radius R_0, this amounts to essentially a predicted linear scaling between flash width and ambient bubble radius.

In both plots, the curves for $N=10^5$ and $N=10^4$ particles were derived by averaging over 10 and 20 simulations, respectively, in order to keep statistical fluctuations to an acceptable level. The $N=10^6$ simulation required just a single simulation for robust statistics.

V. SUMMARY AND FUTURE WORK

Sonoluminescence is well suited to investigation by molecular dynamics because the range of densities and time scales is large, yet the number of particles involved is relatively small. Because this phenomenon still poses experimentally difficult, unsolved questions regarding its mechanism and ultimate energy focusing energy potential, we feel it is an excellent subject for much more detailed MD investigations than the initial effort we have presented here.

In this paper, we introduced a preliminary model for the interior dynamics of single noble gas bubble sonoluminescence, as a hard sphere gas driven by a spherical piston controlled by the Rayleigh-Plesset equation. Energy losses due to ionization were also accounted for using a simplified model. We considered both constant and variable radius hard sphere models, and these lead to quantitatively similar results. Fast, tree-based algorithms allowed us to evolve 10^6 particle systems through the entire collapse process. Our calculations indicate that extreme energy focusing occurs within the bubble, which in some cases is driven by a shocklike compression in the gas. Peak temperatures range from 40 000 K for He to 500 000 K for Xe. These are accompanied by high levels of ionization during the final collapse, and formation of a transient, high-density plasma state seems quite likely.

The imposition of a thermal boundary condition at the wall of the bubble leads to greatly increased energy focusing and nonuniformity within a collapsing bubble. In any case, the predicted flash width scales roughly linearly with the ambient bubble radius.

There are a variety of interesting directions for future research in this problem. For example, our simulations simply treat the bubble wall as a piston moving in with a prescribed velocity. A natural improvement would be to couple the internal molecular dynamics to the wall velocity to obtain a self-consistent bubble motion and internal dynamics. This could be done by coupling to Euler or Navier-Stokes models for the surrounding fluid. This may be particularly important for accurately computing the dynamics through the point of

minimum radius. In our present model there may be overcompression of the gas in some simulations as the minimum radius is approached, since the prescribed piston motion does not respond to the rapid increase in the internal gas pressure. Conversely, when the piston retracts after this point, a nonphysical gap often develops between the bubble boundary and the outer extent of the gas, which may undercompress the gas.

Another important area for future research is adding in water vapor into the bubble interior. This provides a potentially important cooling mechanism, which may strongly modulate the light emission and energy focusing, and may explain the strong ambient temperature dependence of the emitted light intensity. Moreover, it is possible that the water could be directly involved in the light emission (cf. Refs. [22,14,42]). We have done preliminary investigations with water vapor, by allowing water to exit the bubble upon collision with the bubble wall. This preliminary model caused a rapid expulsion of all water vapor from the bubble, suggesting that water evaporation from the bubble surface into the interior should also be included.

Other bubble collapse geometries could also be considered, and these may have different energy focusing characteristics. For example, one could consider a nonspherical collapse, hemispherical bubbles collapsing on a solid surface, or consider collapse geometries appropriate for bubble jetting scenarios. Similarly, one could see if special collapse profiles can be used to reach much higher internal temperatures, and otherwise explore the extremes of the energy focusing potential. Perhaps a mode could even be found in which small amounts of deuterium-deuterium fusion could be induced, assuming there is deuterium gas in the bubble as well.

Including additional atomic physics such as atomic excitation, rotational and vibrational degrees of freedom (needed for non-noble gases or water vapor), and electron-ion recombination would all allow for more accurate energy accounting, and may also be directly related to light emission mechanisms.

Another major direction would be to include electric field effects into the the simulation. Algorithms for such models must treat long range electrostatic interactions to avoid incurring serious errors. They must also be able to evaluate long range forces efficiently since calculating interactions pairwise becomes expensive for more than a few thousand particles. For these reasons, multipole methods are particularly attractive—they use a hierarchy of spatial subdivisions and a multipole expansion to evaluate interactions with little more than linear effort in the number of particles. See Refs. [43,44] for details and see also Ref. [15] for further references on methods for evaluating long range forces. This would potentially allow direct simulation of the ions and electrons produced, which may have an important effect on the dynamics when significant ionization occurs. Moreover, by including atomic excitation, this approach would allow for direct simulation of the light emitting processes. With these effects included, an extremely detailed picture of the SL phenomena could be laid out.

Of course, larger scale, parallel simulations are essential to actually achieve direct comparisons with present SL experiments. Because the simple hard sphere interactions are quite local, the system should be amenable to parallelization. We expect that the cost (in collision count) for a hard sphere MD simulation scales roughly like $N^{4/3}$, where N is the number of particles, since the collapse time from the ambient to the minimum radius scales linearly with R_0 (and so we conjecture that the collision rate also increases roughly linearly with the R_0). Thus simulations using one hundred times as many particles (i.e., $N=10^8$) would require 500 times as much computer time assuming near optimality in the algorithm. This is somewhat beyond the range of a single supercomputer CPU, but would become quite practical on a 100 node system of workstation-grade CPUs.

Finally, it would be of great interest to investigate where less costly continuum models and Monte Carlo simulations are appropriate for studying sonoluminescence and to develop techniques for coupling these methods to detailed molecular dynamics simulations near the light emitting hot spot, in order to produce more complete models with greater predictive validity.

There is also a great deal to explore experimentally. One example relevant to our study is that it would be useful to measure flash width as a function of ambient bubble radius (or, in practice, intensity and frequency of the driving sound field), for comparison with the scaling predictions of MD and other models.

ACKNOWLEDGMENTS

We thank D. B. Hash, A. L. Garcia, and P. H. Roberts for valuable discussions. S.J.R. was partially supported by DARPA and NSERC Canada. S.P. and B.M. were partially supported by DARPA.

[1] H. Frenzel and H. Schultes Z. Phys. Chem. Abt. B **27**, 421 (1934).
[2] P. R. Temple, Master's thesis, University of Vermont, 1970.
[3] D.F. Gaitan and L.A. Crum, J. Acoust. Soc. Am. **91**, 3166 (1992).
[4] B.P. Barber and S.J. Putterman Nature (London), **352**, 318 (1991).
[5] S.J. Putterman and K.R. Weninger, Annu. Rev. Fluid Mech. **32**, 445 (2000).
[6] B.P. Barber, R.A. Hiller, R. Lofstedt, S.J. Putterman, and K.R. Weninger Phys. Rep. **281**, 66 (1997).
[7] S. Hilgenfeldt, S. Grossmann, and D. Lohse, Nature (London), **398**, 402 (1999).
[8] C.C. Wu and P.H. Roberts, Phys. Rev. Lett. **70**, 3424 (1993).
[9] H.P. Greenspan and A. Nadim, Phys. Fluids A **5**, 1065 (1993).
[10] W.C. Moss, D.B. Clarke, and D.A. Young, Science **276**, 1398 (1997).
[11] L. Kondic, J.I. Gersten, and C. Yuan Phys. Rev. E **52**, 4976 (1995).

[12] V.Q. Vuong, A.J. Szeri, and D.A. Young, Phys. Fluids **11**, 10 (1999).
[13] K. Yasui, Phys. Rev. E **56**, 6750 (1997).
[14] W.C. Moss, D.A. Young, J.A. Harte, J.L. Levatin, B.F. Rozsnyai, G.B. Zimmerman, and I.H. Zimmerman, Phys. Rev. E **59**, 2986 (1999).
[15] D. C. Rapaport, *The Art of Molecular Dynamics Simulation* (Cambridge University Press, Cambridge, England, 1998).
[16] K. R. Weninger, C. Camara, and S. J. Putterman, Phys. Rev. E, **63**, 016310 (2001).
[17] M. Woo and I. Greber, AIAA J. **37**, 215 (1999).
[18] S.J. Ruuth, S. Putterman, and B. Merriman, e-print physics/0104062 2001.
[19] B. Metten and W. Lauterborn, in *Nonlinear Acoustics at the Turn of the Millennium: ISNA 15, 15th International Symposium on Nonlinear Acoustics*, edited by W. Lauterborn and T. Kurz, AIP Conf. Proc. No. 524 (AIP, Melville, NY, 2000), pp. 429–432.
[20] B. Metten and W. Lauterborn, Ph.D. thesis, Universität Göttingen, 2001.
[21] B.P. Barber, C.C. Wu, R. Lofstedt, P.H. Roberts, and S.J. Putterman, Phys. Rev. Lett., **72**, 1380 (1994).
[22] S.J. Putterman, P.G. Evans, G. Vazquez, and K. Weninger, Nature (London) **409**, 782 (2001).
[23] G. Vazquez, C. Camara, S.J. Putterman, and K. Weninger, Opt. Lett. **26**, 575 (2001).
[24] G. Vazquez, C. Camara, S. J. Putterman, and K. Weninger, Phys. Rev. Lett. **88**, 197402 (2002).
[25] K.R. Weninger, P.G. Evans, and S.J. Putterman, Phys. Rev. E **61**, 1020 (2000).
[26] W. B. Russel, D. A. Saville, and W. R. Schowalter, *Colloidal Dispersions* (Cambridge University Press, New York, 1989).
[27] G. A. Bird, *Molecular Gas Dynamics and the Direct Simulation of Gas Flows* (Oxford University Press, New York, 1998).
[28] R. Lofstedt, B.P. Barber, and S.J. Putterman, Phys. Fluids A **5**, 2911 (1993).
[29] J. H. Jeans, *Introduction to the Kinetic Theory of Gases* (Cambridge University Press, Cambridge, England, 1940).
[30] A.O. Rankine, Proc. R. Soc. London, Ser. A **83**, 516 (1910).
[31] A.O. Rankine, Proc. R. Soc. London, Ser. A **84**, 181 (1910).
[32] G.A. Bird, Prog. Astronaut. Aeronaut. **74**, 239 (1981).
[33] K. Koura and H. Matsumoto, Phys. Fluids A **3**, 2459 (1991).
[34] K. Koura and H. Matsumoto, Phys. Fluids A **4**, 1083 (1992).
[35] H.A. Hassan and D.B. Hash, Phys. Fluids A **5**, 738 (1993).
[36] S. Chapman and T. G. Cowling, *The Mathematical Theory of Non-Uniform Gases*, 3rd ed. (Cambridge University Press, Cambridge, England, 1970).
[37] *Handbook of Chemistry and Physics*, edited by R. C. West (CRC Press, Boca Raton, 1985).
[38] T.A. Carlson Jr., C.W. Nestor, and N. Wasserman, At. Data **2**, 63 (1970).
[39] J. J. Erpenbeck and W. W. Wood, in *Modern Theoretical Chemistry*, edited by B. J. Berne (Plenum, New York, 1977), Vol. 6B, pp. 1-40.
[40] D.C. Rapaport, J. Comput. Phys. **34**, 184 (1980).
[41] D. E. Knuth, *Sorting and Searching*, Vol. 3 of *The Art of Computer Programming* (Addison-Wesley, Reading, MA, 1973).
[42] G. Vazquez and S.J. Putterman, Phys. Rev. Lett. **85**, 3037 (2000).
[43] L. Greengard and V. Rokhlin, J. Comput. Phys. **73**, 325 (1987).
[44] L. Greengard, *The Rapid Evaluation of Potential Fields in Particle Systems* (MIT Press, Cambridge, 1988).